

Radar Backscatter Measurement Accuracy for a Spaceborne Pencil-Beam Wind Scatterometer with Transmit Modulation

David G. Long, *Member, IEEE*, and Michael W. Spencer

Abstract—Scatterometers are remote sensing radars designed to measure near-surface winds over the ocean. The difficulties of accommodating traditional fan-beam scatterometers on spacecraft has led to the development of a scanning pencil-beam instrument known as SeaWinds. SeaWinds will be part of the Japanese Advanced Earth Observing Satellite II (ADEOS-II) to be launched in 1999. To analyze the performance of the SeaWinds design, a new expression for the measurement accuracy of a pencil-beam system is required. In this paper we derive a general expression for the backscatter measurement accuracy for a pencil-beam scatterometer which includes the effects of transmit signal modulation with simple power detection. Both separate and simultaneous signal+noise and noise-only measurements are considered. The utility of the new expression for scatterometer design tradeoffs is demonstrated using a simplified geometry. A separate paper [8] describes detailed tradeoffs made to develop the SeaWinds design.

Index Terms—Scatterometry, SeaWinds, wind measurement.

I. INTRODUCTION

A SCATTEROMETER is a radar system that measures the radar backscatter coefficient, σ^o , of an illuminated surface. The scatterometer transmits a series of RF pulses and measures the total power (energy) of the backscattered signal which is corrupted by noise. A separate measurement of the noise-only power is subtracted from this measurement to yield the return signal energy. Using the well-known radar equation [Sec. 7, 9] and the measurement geometry, the backscatter energy measurements are converted into σ^o measurements. Multiple measurements of σ^o from different azimuth and/or incidence angles are used to infer the wind direction. Naderi *et al.* [7] provides a recent review of scatterometry with emphasis on the NASA Scatterometer (NSCAT) instrument.

NSCAT is an example of a fan-beam Doppler scatterometer which requires multiple large antennas (3 m long) to achieve the required fan-beam illumination pattern. The field-of-view requirements of the antennas are very strict making fan-beam scatterometers very difficult to accommodate on spacecraft. In addition, complicated onboard processors are required to achieve a low data rate.

Scanning pencil-beam scatterometers offer an alternative design concept which can result in smaller, lighter instruments with simpler field-of-view requirements [3]. Further, because the antenna illumination is concentrated in a smaller area, a much higher signal-to-noise ratio (SNR) can be obtained with a smaller transmitter, resulting in reduced power requirements. Complicated signal processing is not required and the data rate is small. As a result, a pencil-beam scatterometer can be more easily accommodated on spacecraft than a fan-beam. (More exhaustive comparisons of fan-beam and pencil-beam scatterometers are contained in [3] and [6], and in a companion paper [8].)

A key difference between fan-beam and pencil-beam scatterometers is measurement dwell time. Fan-beam scatterometers provide long dwell times, albeit a reduced SNR compared to the higher SNR, but shorter dwell time of the pencil-beam scatterometer system. For interrupted CW operation, fan-beam Doppler scatterometers tend to provide higher time-bandwidth products. However, the transmit signal of a pencil-beam scatterometer can be modulated to improve the time-bandwidth product. In either case, a key design goal is to optimize the σ^o measurement accuracy within the design constraints.

A common metric for evaluating the accuracy of the σ^o measurement is the so-called K_p parameter [1], [2], [5]. K_p is the normalized standard deviation of σ^o measurement

$$K_p = \frac{\sqrt{\text{var}\{\sigma_{\text{meas}}^o\}}}{\sigma^o}.$$

A general goal in scatterometer design is to minimize the measurement K_p . Further, the measurement K_p is also used in the processing of the the σ^o measurements into winds [7].

Expressions for K_p for Doppler fan-beam scatterometers such as the Seasat scatterometer (SASS) and the NSCAT with its digital processor have previously been derived [1], [2]. These expressions are for an interrupted-CW transmit signal. A general expression for a modulated transmit signal is required for analyzing the performance of a pencil-beam scatterometer.

In this paper we develop a K_p expression for pencil-beam scatterometers which includes transmit signal modulation and a simple total power (energy) detection scheme. To derive this expression we begin with an expression for the return echo, consider the method for estimating the signal energy, and derive the general K_p expression. We then relate the K_p expression to the radar ambiguity function for a simplified

Manuscript received September 21, 1995; revised May 15, 1996.

D. G. Long is with the Electrical and Computer Engineering Department, Brigham Young University, Provo UT 84602 USA.

M. W. Spencer is with the Jet Propulsion Laboratory, California Institute of Technology, Pasadena, CA 91109 USA.

Publisher Item Identifier S 0196-2892(97)00967-4.

measurement geometry. This enables tradeoffs in the choice of modulation function to minimize K_p which are discussed. Finally, a summary conclusion is presented. A separate paper [8] describes the use of the general K_p expression to make tradeoffs in the design of SeaWinds. Some detailed derivations are contained in the Appendix.

II. RETURN ECHO (SIGNAL) MODELING

The scatterometer transmits a series of radar pulses and measures the return echo energy. In this section we develop an expression for the return echo given a modulated transmit signal. We first consider the response from a point-target response and extend this to the response from a distributed target. Adopting a complex exponential formulation for the carrier to simplify the discussion, the transmitted radar signal, $\xi_t(t)$, for a single pulse can be written in the form,

$$\xi_t(t) = \sqrt{E_t} a(t) e^{j\omega_c t}$$

where t is time, E_t is the total transmitted energy for a single pulse, $\omega_c = 2\pi f_c$ where f_c is the carrier frequency, and $a(t)$ is the carrier modulation function. The pulse repetition period is T_i and pulse length is T_p . For modeling purposes, $a(t) = 0$ for $t < 0$ and $a(t) = 0$ for $t > T_p$. The complex modulation function $a(t)$ is normalized so that

$$\int_0^{T_p} |a(t)|^2 dt = 1.$$

Let B_a be the bandwidth of $a(t)$. We assume that $B_a \ll f_c$.

Consider the return echo $\xi_p(t)$ from a point scatterer on the Earth's surface. The scatterometer is moving at a constant velocity. Fig. 1 shows the antenna illumination geometry for a conically-scanning pencil-beam scatterometer system. For a spaceborne scatterometer the return echo from a point target can be approximated by a time-delayed, Doppler-shifted replica of the transmit pulse scaled by antenna gain and spreading term, i.e.,

$$\xi_p(t) = V_p e^{j\phi_p} \frac{\sqrt{E_t} G(x, y) \lambda}{(4\pi)^{3/2} r^2(x, y)} a(t - 2r(x, y)/c) \cdot e^{-j\omega_d(x, y)t} e^{-j2\omega_c r(x, y)/c} e^{j\omega_c t}$$

where c is the speed of light, $r(x, y)$ is the slant range to the target at cross track location x and along-track location y , $\omega_d = 2v_r/c$ is the the Doppler shift due to the relative velocity v_r between the target on the surface and spacecraft, $G(x, y)$ is the antenna gain in the direction of the target, λ is the radar wavelength, and $V_p e^{j\phi_p}$ is the magnitude and phase of the point target response.

For large spatially distributed targets, such as the ocean, the return echo $\xi_s(t)$ can be modeled as the superposition of the echo from a very large number of point targets. For a typical spaceborne scatterometer operating at microwave frequencies, the superposition can be expressed as an area integral [Sec. 7, 9] given in (1), shown at the bottom of the next page, where $V(x, y) e^{j\phi(x, y)}$ is the effective response from a large number of point scatterers within the differential area dA which we assume is larger than the correlation length of

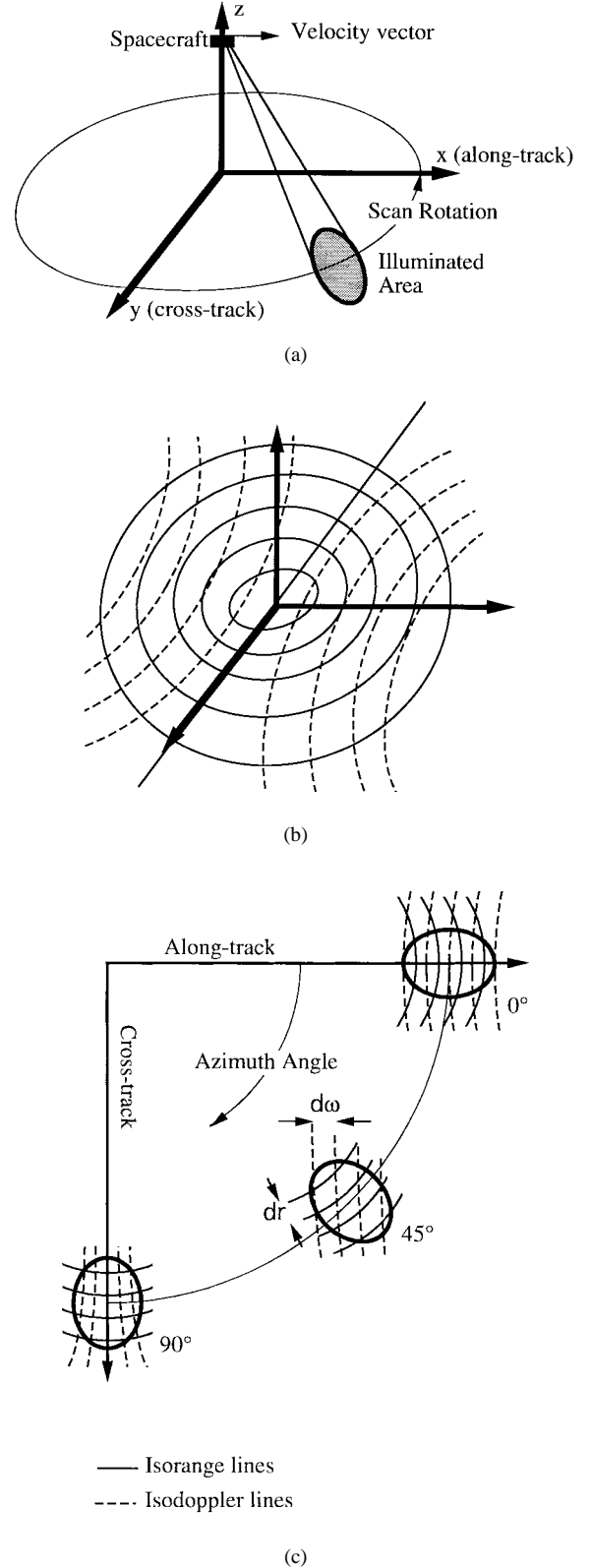


Fig. 1. Geometry of a conically scanning spaceborne pencil-beam scatterometer. (a) Scanning geometry. (b) Isodoppler and isorange lines. (c) Isodoppler and isorange lines for several cell locations along the scan.

the ocean's surface at the frequency f_c . It follows from the central limit theorem that the real and imaginary components of the sum of scatterers may be assumed to be independent,

normally distributed random variables [Sec. 7, 9]. Assuming homogeneity, the second moment of V_s can be related to the normalized radar cross section σ^o

$$\mathcal{E}[V_s^2(x, y)] = A_r(x, y)\sigma^o \quad (2)$$

where \mathcal{E} denotes statistical expectation and A_r is the area of the differential element over which the integration is performed. Because of the short correlation length of the surface, V_s and ϕ_s are independent for each differential element. We will assume that σ^o is constant over the illuminated area.

We will find it convenient to express the area integral in (1) in terms of the Doppler shifts and the slant range, i.e., (3), shown at the bottom of the pagewhere we have removed the carrier frequency. For a spaceborne scatterometer the denominator r^2 can be assumed to be approximately constant over the integral. Let \bar{r} be the mean value of r over the integral. Equation (3) then becomes

$$\xi_s(t) \approx \sqrt{\frac{E_t \lambda^2}{(4\pi)^3 \bar{r}^4}} \int_{r, \omega_d} G(r, \omega_d) a(t - 2r/c) \cdot e^{-j\omega_d t} e^{j2\omega_c r/c} V_s(r, \omega_d) e^{-j\phi_s(r, \omega_d)} dr d\omega_d.$$

We now develop some results which will be used later. Using (2) it can be shown that

$$\mathcal{E}[|\xi_s(t)|^2] = X \sigma^o K_a(t) \quad (4)$$

where $K_a(t)$ is the weighted modulation correlation function defined as

$$K_a(t) = \frac{1}{G_0^2 A_c} \int_{r, \omega_d} |a(t - 2r/c)|^2 G^2(r, \omega_d) \cdot A_r(r, \omega_d) dr d\omega_d, \quad (5)$$

X is defined as

$$X = \frac{E_t \lambda^2 G_0^2 A_c}{(4\pi)^3 \bar{r}^4}.$$

G_0 is the peak antenna gain over the footprint, and A_c is the effective cell area defined as

$$A_c = \frac{1}{G_0^2} \int_{r, \omega_d} G^2(r, \omega_d) A_r(r, \omega_d) dr d\omega_d.$$

It can be shown that

$$\mathcal{E}[|\xi_s(t)|^2 |\xi_s(\tau)|^2] = X^2 \sigma^{o2} [K_a(t)K_a(\tau) + J_a(t, \tau)]$$

where $J_a(t, \tau)$ is the two-dimensional weighted modulation cross-correlation function defined as

$$J_a(t, \tau) = \frac{1}{G_0^4 A_c^2} \int \cdots \int a(t - 2r/c) a^*(\tau - 2r/c) \cdot a^*(t - 2r'/c) a(\tau - 2r'/c) \cdot G^2(r, \omega_d) G^2(r', \omega'_d) A_r(r, \omega_d) A_r(r', \omega'_d) \cdot e^{-j(\omega_d - \omega'_d)(t - \tau)} dr d\omega_d dr' d\omega'_d \quad (6)$$

and that

$$\mathcal{E}[\xi_s(t) \xi_s^*(\tau)] = X \sigma^o L_a(t, \tau)$$

where $L_a(t, \tau)$ is the weighted time correlation function defined as

$$L_a(t, \tau) = \frac{1}{G_0^2 A_c} \int_{r, \omega_d} a(t - 2r/c) a^*(\tau - 2r/c) \cdot e^{-j\omega_d(t - \tau)} G^2(r, \omega_d) A_r(r, \omega_d) dr d\omega_d. \quad (7)$$

We note that since $\mathcal{E}\{[V_s(r, \omega_d) e^{j\phi_s(r, \omega_d)}]^2\} = 0$ it can be shown that $\mathcal{E}[\xi_s(t) \xi_s(\tau)] = \mathcal{E}[\xi_s^*(t) \xi_s^*(\tau)] = 0$. These facts are used in later derivations.

III. ECHO SIGNAL ENERGY ESTIMATION

Ultimately, we want to estimate the surface σ^o . This estimate is obtained by processing the received echo. Unfortunately, the return echo is corrupted by additive thermal noise. The received radar signal $\xi_{sn}(t)$ consists of the return echo with additive noise $\nu(t)$ due to thermal noise in the receiver and the communication channel, i.e.,

$$\xi_{sn}(t) = \xi_s(t) + \nu(t)$$

We assume that the down-converted return echo $\xi_s(t)$ (signal) and noise $\nu(t)$ are independent and that the noise is a real white process with a power spectral density of $n_0/2$ over the measurement bandwidth. The signal+noise measurement bandwidth is B_r ($B_r > B_a$). The noise-only measurement is made over the bandwidth B_n . In the following analysis we assume ideal filters for simplicity.

To estimate σ^o , a measurement of the signal energy (total power) is made by subtracting a "noise-only" measurement from the signal+noise measurement. The noise-only and signal+noise may be made separately (as done by SASS and NSCAT) or they may be made simultaneously (planned for

$$\begin{aligned} \xi_s(t) &= \int \xi_p(t) dA \\ &= \frac{\sqrt{E_t} \lambda}{(4\pi)^{3/2}} \int \frac{G(x, y) a(t - 2r(x, y)/c) e^{-j\omega_d(x, y)t} e^{j2\omega_c r(x, y)/c} V_s(x, y) e^{j\phi_s(x, y)}}{r^2(x, y)} e^{j\omega_c t} dA \end{aligned} \quad (1)$$

$$\xi(t) = \sqrt{\frac{E_t \lambda^2}{(4\pi)^3}} \int_{r, \omega_d} \frac{G(r, \omega_d) a(t - 2r/c) e^{-j\omega_d t} e^{j2\omega_c r/c} V_s(r, \omega_d) e^{-j\phi_s(r, \omega_d)}}{r^2} dr d\omega_d. \quad (3)$$

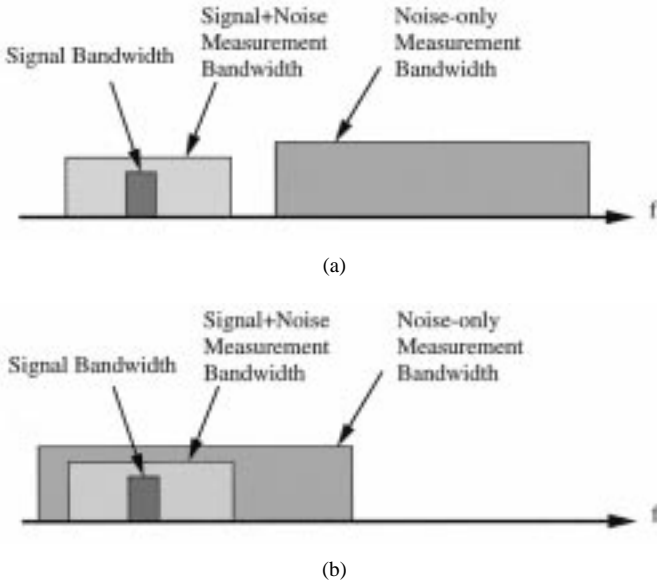


Fig. 2. Two cases for simultaneous Signal+Noise and Noise-only measurements. (a) Disjoint measurement bandwidths. Measurements are independent and noise-only measurement bandwidth contains no signal; (b) noise-only measurement bandwidth includes echo signal.

SeaWinds). When the measurements are made simultaneously, minimum K_p for a fixed noise-only bandwidth dictates that the bandwidths be distinct [refer to Fig. 2(a)]. This results in independent signal+noise and noise-only measurements. However, when the signal+noise and noise-only bandwidths overlap [refer to Fig. 2(b)], the measurements are correlated and the effective K_p is increased. Nevertheless, simultaneous measurements with overlapping bandwidths may be easier to implement in hardware (see [8]).

In any case, σ^o is inferred from the estimated signal energy. Accurately estimating the signal energy is thus essential to accurately determining σ^o . The accuracy of the estimate is quantified by K_p .

In the following sections we consider the σ^o estimation algorithm, the signal energy estimation algorithm, and derive the signal K_p for the case when the signal+noise and noise-only measurements are independent. The K_p for the overlapped bandwidth case is derived in the appendix.

A. σ^o Estimation

To estimate σ^o , measurements of the signal+noise (C_{sn}) and the noise-only (C_{no}) are made. A signal estimate \widehat{E}_s is formed as a linear combination of C_{sn} and C_{no} , i.e.

$$\widehat{E}_s = a_1 C_{sn} + b_1 C_{no} \quad (8)$$

where C_{sn} , C_{no} , a_1 , and b_1 are described below. An estimate $\widehat{\sigma^o}$ of σ^o is formed from \widehat{E}_s as

$$\widehat{\sigma^o} = \frac{1}{X} \widehat{E}_s = \frac{a_1}{X} \left[C_{sn} + \frac{b_1}{a_1} C_{no} \right] = \frac{a_1}{X} [C_{sn} + c_1 C_{no}]$$

where $c_1 = a_1/b_1$. By proper choice of a_1 and b_1 , the energy estimate is unbiased, i.e., $E_s = \mathcal{E}[\widehat{E}_s]$. Note that $K_p[\widehat{\sigma^o}] = K_p[\widehat{E}_s]$. In the following section K_p is computed

by first determining the variance of C_{sn} and C_{no} and then using (8).

B. Energy Estimation

While there are a variety of possible signal processing and estimation techniques which can be used to obtain C_{sn} and C_{no} , these are limited by practical considerations. For example, the time and frequency dispersion in the echo makes a matched filter detection very complex and unsuited for onboard processing. Instead, a less optimum, though very simple, detection scheme is employed (see Fig. 3) with

$$C_{sn} = \int_{T_1}^{T_2} |\xi_{sn}(t) * h(t)|^2 dt \quad (9)$$

$$C_{no} = \int_{T_3}^{T_4} |\nu(t) * h_n(t)|^2 dt. \quad (10)$$

If the bandwidth of $H(\omega)$ is sufficiently wide, the filter does not affect the signal component of $\xi_{sn}(t)$. In this case the signal+noise measurement of (9) can be expressed as

$$C_{sn} = C_s + C_n + C_c \quad (11)$$

where C_s is the signal energy, C_n is the noise energy, and C_c is the signal and noise cross product, i.e.,

$$\begin{aligned} C_s &= \int_{T_1}^{T_2} |\xi_s(t)|^2 dt \\ C_n &= \int_{T_1}^{T_2} |\nu(t) * h(t)|^2 dt \\ C_c &= \int_{T_1}^{T_2} \{ \xi_s(t) [\nu^*(t) * h^*(t)] \\ &\quad + \xi_s^*(t) [\nu(t) * h(t)] \} dt. \end{aligned} \quad (12)$$

This decomposition simplifies computing the variance of C_{sn} .

Noting the independence of the signal and noise and using the fact that the noise is Gaussian, it can be shown (with some effort) that the expected value of the third term of (11) is zero, i.e. $\mathcal{E}[C_c] = 0$. Thus,

$$\mathcal{E}[C_{sn}^2] = \mathcal{E}[(C_s + C_n)^2] + \mathcal{E}[C_c^2]. \quad (13)$$

In order to compute $\text{var}[C_c]$ we note that

$$\begin{aligned} \mathcal{E}[\xi_s(t) \nu(t) \xi_s^*(\tau) \nu^*(\tau)] \\ &= \mathcal{E}[\xi_s(t) \xi_s^*(\tau)] \mathcal{E}[\nu(t) \nu^*(\tau)] \\ &= R_s(t, \tau) R_\nu(t - \tau) \end{aligned}$$

where

$$\begin{aligned} R_s(t, \tau) &= X \sigma^o L_a(t, \tau) = E_s L_a(t, \tau) \\ R_\nu(t - \tau) &= 2B_r \frac{n_0}{2} \text{sinc}(2B_r[t - \tau]). \end{aligned}$$

Since $\nu(t)$ is real and $\mathcal{E}[\xi_s(t) \xi_s(\tau)] = \mathcal{E}[\xi_s(t) \xi_s^*(\tau)] = 0$, the unconjugated cross products drop out. It can then be shown that

$$\text{var}[C_c] = E_s^2 S U \quad (14)$$

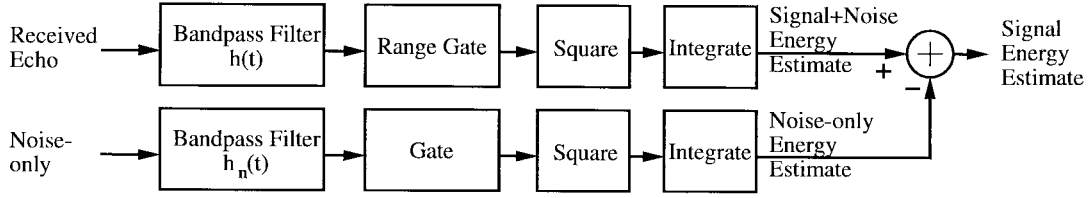


Fig. 3. Echo total power (energy) detection scheme.

where S is noise-to-signal ratio

$$S = \frac{1}{E_s} \left(2T_r B_r \frac{n_0}{2} \right)$$

and [see (7)]

$$U = \frac{2}{T_r} \int_{T_1}^{T_2} \int_{T_1}^{T_2} \text{Re}[L_a(t, \tau)] \text{sinc}[2B_r(t - \tau)] dt d\tau. \quad (15)$$

For the first term of (11), (4) can be used to compute the expected value of C_s

$$\mathcal{E}[C_s] = X\sigma^o \int_{T_1}^{T_2} K_a(t) dt = \frac{X\sigma^o}{a_1} \triangleq E_s/a_1$$

where the energy normalization coefficient a_1 is defined as [see (5)]

$$a_1 = \left[\int_{T_1}^{T_2} K_a(t) dt \right]^{-1}. \quad (16)$$

The noise-free signal variance (due to Rayleigh fading) is then

$$\text{var}[C_s] = \mathcal{E}[C_s^2] - \mathcal{E}^2[C_s] = E_s^2 V \quad (17)$$

where the normalized signal variance V is defined as [see (6)]

$$V = \int_{T_1}^{T_2} \int_{T_1}^{T_2} J_a(t, \tau) dt d\tau. \quad (18)$$

The noise-free measurement K_p , denoted by K'_p , is then

$$K'_p = a_1 \sqrt{V} \quad (19)$$

Assuming ideal low-pass filters, the statistics of the second term of (11) and the noise-only estimate of (10) are [2]

$$\begin{aligned} \mathcal{E}[C_n] &= 2B_r T_r \frac{n_0}{2} \triangleq E_n \\ \text{var}[C_n] &= \left(2T_r B_r \frac{n_0}{2} \right)^2 2I(2B_r T_r) \end{aligned} \quad (20)$$

$$\begin{aligned} \mathcal{E}[C_{no}] &= 2B_n T_n \frac{n_0}{2} = \frac{B_n T_n}{B_r T_r} E_n \\ \text{var}[C_{no}] &= \left(2T_n B_n \frac{n_0}{2} \right)^2 2I(2T_n B_n) \end{aligned} \quad (21)$$

where $T_r = T_2 - T_1$, $T_n = T_4 - T_3$, and the function $I(p)$ is defined as [2]

$$I(p) = 2 \int_0^1 (1 - \alpha) \left(\frac{\sin \pi p \alpha}{\pi p \alpha} \right)^2 d\alpha. \quad (22)$$

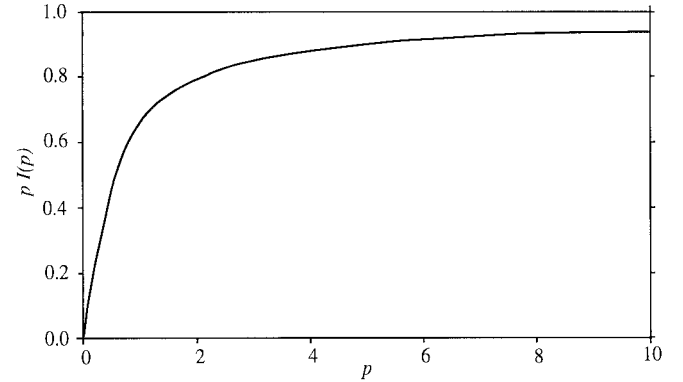


Fig. 4. Plot of $pI(p)$.

A plot of $pI(p)$ is shown in Fig. 4. Note that for large p (corresponding to large time-bandwidth products), $pI(p) \rightarrow 1$.

To obtain unbiased measurements the noise-only estimation coefficient b_1 is selected as,

$$b_1 = a_1 \frac{B_r T_r}{B_n T_n}$$

so that $\mathcal{E}[a_1 C_n - b_1 C_{no}] = 0$.

C. Computing K_p

Since the signal is independent of the noise and the noise is zero mean

$$\mathcal{E}[C_{sn}] = \mathcal{E}[C_s] + \mathcal{E}[C_n] = \frac{E_s}{a_1} + 2B_r T_r \frac{n_0}{2}.$$

Using this result, (13), and the fact that $\mathcal{E}[C_c] = 0$, it follows that

$$\text{var}[C_{sn}] = \text{var}[C_s] + \text{var}[C_n] + \text{var}[C_c].$$

With this result and (14), (17), (20), (21), we obtain,

$$\text{var}[C_{sn}] = E_s^2 V + E_s^2 S U + 2I(2T_r B_r) \left(2T_r B_r \frac{n_0}{2} \right)^2. \quad (23)$$

Using the definitions of a_1 and b_1 it follows that

$$\mathcal{E}[\widehat{E}_s] = \mathcal{E}[a_1 C_{sn} - b_1 C_{no}] = a_1 \mathcal{E}[C_s] = X\sigma^o = E_s$$

and

$$\text{var}[\widehat{E}_s] = a_1^2 E_s^2 \{ V + S U + 2S^2 [I(2T_r B_r) + I(2T_n B_n)] \}.$$

The K_p of the noisy signal energy estimate is then

$$K_p[\widehat{E}_s] = a_1 \{V + SU + 2S^2[I(2T_r B_r) + I(2T_n B_n)]\}^{1/2}. \quad (24)$$

For multiple independent pulses this becomes

$$K_p[\widehat{E}_s] = \frac{a_1}{\sqrt{N_p}} \{V + SU + 2S^2[I(2T_r B_r) + I(2T_n B_n)]\}^{1/2} \quad (25)$$

which is our final result for distinct signal+noise and noise-only measurements. In this equation S is the noise-to-signal ratio, T_r is the signal range gate length, T_n is the noise-only measurement length, B_r is the signal measurement bandwidth, B_n is the noise-only measurement bandwidth, and N_p is the number of pulses. As noted earlier $I(x) \approx 1/x$ for $x \gg 1$. The energy normalization coefficient a_1 is a function of the modulation, the range geometry, the antenna pattern, and the signal range gate [(5) and (16)]. The normalized signal variance term V is a rather complicated function of the modulation, the range and Doppler geometry, the antenna pattern, and the signal range gate [(6) and (18)]. The signal and noise cross-term U depends on the signal measurement bandwidth, the range and Doppler geometry, the antenna pattern, and the signal range gate [(7) and (15)]. In effect, V is the contribution of the signal power variance, SU is the contribution of the signal and noise covariance, and the S^2 term is the contribution of the noise variance.

In the appendix it is shown that for interrupted CW operation (no modulation) with a simplified geometry and antenna pattern

$$\begin{aligned} a_1 &= 1 \\ V &= \frac{1}{T_p B_D} \frac{T_r}{T_p} \approx \frac{1}{T_p B_D} \\ U &= \frac{2}{T_p B_D} \end{aligned}$$

where B_D is the Doppler bandwidth. Equation (25) is then equivalent to Fisher's K_p expression (see (48) in [2]). When modulation is employed, it is shown in Section IV-A that for a simplified geometry a_1 and V can be expressed in terms of the radar ambiguity function defined by the modulation function: a_1^{-1} is the radar ambiguity function evaluated at the origin and V is a weighted integral of the radar ambiguity function. As discussed in Section IV, choosing an appropriate modulation function can reduce K_p by reducing V .

D. K_p for Overlapping Bandwidths and Simultaneous Measurements

Some hardware complexity reduction can be obtained by making simultaneous signal+noise and noise-only measurements. If the bandwidths are distinct and filter sidelobes are neglected the measurements are independent and (25) can be used. However, when the bandwidths overlap and the signal is contained within the "noise-only" measurement bandwidth (refer to Fig. 2) additional terms in the K_p expression arise due

to cross correlation between the signal+noise and "noise-only" measurements. For the case of simultaneous measurements with overlapping bandwidths (SMBW) the K_p expression is

$$K_p[\widehat{E}_s(\text{SMBW})] = \frac{a_1}{\sqrt{N_p}} \{V + S(U + W) + 2S^2[Q_1 I(2B_r T_r) + Q_2 I(2B_n T_r)]\}^{1/2} \quad (26)$$

where

$$W = (U' - U) \frac{B_r^2}{(B_n - B_r)^2} \quad (27)$$

$$Q_1 = 1 - \frac{B_r^2}{(B_n - B_r)^2} \quad (28)$$

$$Q_2 = \frac{B_n^2}{(B_n - B_r)^2} \quad (29)$$

and U' is defined similar to (15) but with B_r replaced by B_n . Equation (26) is derived in Appendix A.

IV. K_p VERSUS $a(t)$

Equations (25) and (26) provide analytic expressions for K_p when the transmit signal is modulated. In this section we consider the effects of the choice of $a(t)$ on K_p . We will show that for some measurement geometries K_p can be improved by using a wideband $a(t)$; however, we note that, depending on the choice of $a(t)$, K_p may increase for some geometries.

Note that the normalized signal variance term V in the K_p expressions [(25) and (26)] corresponds to the variability due only to the signal while the U term arises from cross products of the signal and noise. Also note that the S^2 term is not affected by the choice of $a(t)$ (other than by the possible need to increase B_r to insure processing of the complete signal bandwidth). With these in mind we will consider just the effect of the choice of $a(t)$ on the noise-free K_p, K'_p , given by (19).

In order to gain some insight into the effects of different modulation functions on K_p , we assume a simplified geometry and antenna illumination pattern to relate the K_p to the radar ambiguity function $X_a(\tau, \nu)$, defined as

$$X_a(\tau, \nu) = \int_{-\infty}^{\infty} a(t) a^*(t + \tau) e^{j2\pi\nu t} dt. \quad (30)$$

The radar ambiguity function arises from matched filter considerations and is widely used in surveillance radar systems performance analysis.

A. K'_p and the Radar Ambiguity Function

In principle each term of the K_p equation has to be evaluated separately for each different observation geometry. Because exact expressions are very complicated, (the full expression is evaluated for SeaWinds in the companion paper [8]) a simplified analysis is used in this section to provide insight into the tradeoff between K_p and $a(t)$. For the simplified analysis a simplified geometry for the isorange and isodoppler lines

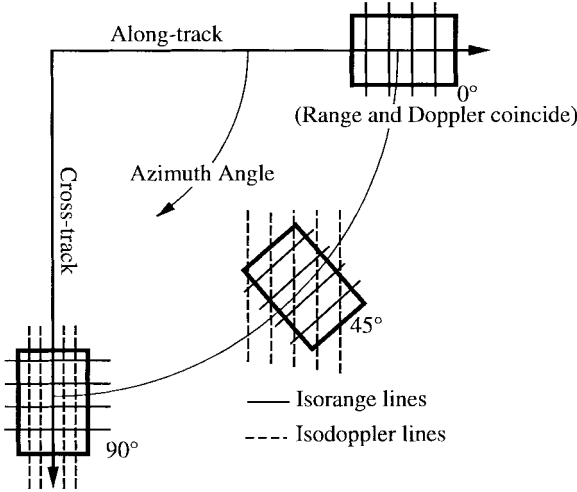


Fig. 5. Simplified cell illumination geometry and isolines. (Compare with Fig. 1)

is assumed (see Fig. 5). A simplified antenna pattern is also assumed,

$$G(r, \omega_d) = \begin{cases} G_0 & r, \omega_d \in \text{illuminated rectangle} \\ 0 & \text{else.} \end{cases}$$

With these simplifications, the area function $A_r(r, \omega_d)$ in the V integral in (18) can be pulled out. Let us consider two cases. Case one corresponds to a 90° azimuth angle while case two corresponds to a 0° azimuth angle. For case one (azimuth angle of 90°) the integral in (3) reduces to two integrations in r and ω_d with

$$A_r(r, \omega_d) = \frac{A_c}{\Delta r \omega_D}$$

where $\Delta r = r_x - r_n$ is the difference between the maximum range r_x and the minimum range r_n over the footprint and $\omega_D = \omega_x - \omega_n$ is the difference between the maximum Doppler ω_x and the minimum Doppler ω_n over the footprint. For later use we assign $\omega_c = \omega_x + \omega_n$ which is the Doppler center frequency and set $\alpha = 2/c$ and $T_c = \alpha \Delta r$.

For case two (azimuth angle of 0°), ω_d and r coincide and the integral in (3) effectively reduces to a line integral. Choosing r as the independent variable,

$$A_r(r, \omega_d) = \frac{A_c}{\Delta r}$$

with $\omega_d = \beta r + \gamma$ where $\beta = \omega_D / \Delta r$ and $\gamma = \omega_c - \omega_D / 2$ are constants. We consider each case in greater detail below.

1) *Case 1, 90° Azimuth:* For the case one simplified geometry a_1^{-1} and V are

$$a_1^{-1} = \frac{1}{\omega_D \Delta r} \int_{T_1}^{T_2} \int_{r_n}^{r_x} \int_{\omega_n}^{\omega_x} |a(t - r\alpha)|^2 dr d\omega_d dt \quad (31)$$

$$V = \frac{1}{\omega_D^2 \Delta r^2} \int_{T_1}^{T_2} \int_{T_1}^{T_2} \int_{r_n}^{r_x} \int_{r_n}^{r_x} \int_{\omega_n}^{\omega_x} \int_{\omega_n}^{\omega_x} a(t - r\alpha) a^*(\tau - r\alpha) a^*(t - r'\alpha) a(\tau - r'\alpha) \cdot e^{-j(\omega_d - \omega'_d)(t - \tau)} dr d\omega_d dr' d\omega'_d dt d\tau. \quad (32)$$

To simplify these expressions, consider the integral

$$\int_{T_1}^{T_2} a(\tau - r'\alpha) a^*(\tau - r\alpha) e^{j\omega\tau} d\tau.$$

Using the substitutions $y = t - \alpha r'$ and $\rho = \alpha(r' - r)$ this becomes

$$e^{j\omega\alpha r'} \int_{T_1'}^{T_2'} a(y) a^*(y + \rho) e^{j\omega y} dy \quad (33)$$

where $T_1' = T_1 - \alpha r'$ and $T_2' = T_2 - \alpha r'$. Noting that $a(t)$ is zero outside of the pulse and assuming that the range gates are sufficiently wide to admit all of the echo signal, the limits on the integral in (33) can be extended to infinity, i.e., $T_1' = -\infty$ and $T_2' = +\infty$, without affecting the value of the integral. With this extension the integral in (33) is equivalent to the radar ambiguity function defined in (30). With this extension and assuming that $a(t)$ is symmetric it can then be shown that V can be written as

$$V = \frac{1}{\omega_D^2 T_c^2} \int_{-T_c}^{T_c} \int_{-\omega_D}^{\omega_D} (T_c - |x|) \cdot (\omega_D - |\omega|) |X_a(x, \omega)|^2 dx d\omega.$$

Using the limit extension again it can be shown that, $a_1^{-1} = X_a(0, 0)$. It then follows that the noise-free K_p is

$$K_p'(case 1) = a_1 \sqrt{V} = Y_1(X_a) \quad (34)$$

where $Y_1(X_a)$ (shown at the bottom of the page) is introduced to denote K_p' as a function of the transmit signal modulation for measurement geometry case one.

Equation (34) suggests that K_p' (and therefore V) can be computed as a weighted double integral of the radar ambiguity function. This makes possible (at least for the simplified geometry assumed here) to make analytic tradeoffs between the choice of $a(t)$ and K_p' by computing the ambiguity function for a given modulation function. This will be considered later.

2) *Case 2, 0° Azimuth:* For the case two simplified geometry, a_1^{-1} and V are [compare (31) and (32)]

$$a_1^{-1} = \frac{1}{\Delta r} \int_{T_1}^{T_2} \int_{r_n}^{r_x} |a(t - r\alpha)|^2 dr dt$$

$$V = \frac{1}{\Delta r^2} \int_{T_1}^{T_2} \int_{T_1}^{T_2} \int_{r_n}^{r_x} \int_{r_n}^{r_x} a(t - r\alpha) \cdot a^*(\tau - r\alpha) a^*(t - r'\alpha) a(\tau - r'\alpha) \cdot e^{-j\beta(r - r')(t - \tau)} dr dr' dt d\tau.$$

$$Y_1(X_a) = \frac{1}{X_a(0, 0)} \sqrt{\frac{1}{\omega_D^2 T_c^2} \int_{-T_c}^{T_c} \int_{-\omega_D}^{\omega_D} (T_c - |x|) (\omega_D - |\omega|) |X_a(t, \omega)|^2 dx d\omega}$$

Using previous results, the integral extension idea, and a bit of tedious algebra it can be shown that V can be written as

$$V = \frac{1}{T_c} \int_{-T_c}^{T_c} (T_c - |y|) |X_a(y, \beta y/\alpha)|^2 dy.$$

Similarly, $a_1^{-1} = X_a(0, 0)$, from which it follows that

$$K'_p(\text{case 2}) = a_1 \sqrt{V} = Y_2(X_a) \quad (35)$$

where

$$Y_2(X_a) = \frac{1}{X_a(0, 0)} \sqrt{\frac{1}{T_c^2} \int_{-T_c}^{T_c} (T_c - |y|) |X_a(y, \beta' y)|^2 dy}.$$

is introduced to denote K'_p as a function of the transmit signal modulation for measurement geometry case two.

Again, we see that K'_p is a weighted integral of the radar ambiguity function. However, while case one is a normalized volume integral, case two is a normalized integral along a diagonal slice through the ambiguity function. Depending on the structure of the ambiguity function, the values of the normalized integrals may be quite different. Thus, the measurement geometry can have a significant effect on K'_p and, therefore, on the choice of the modulation function.

B. The Relationship of the Ambiguity Function and K'_p

Equations (34) and (35) suggest that the noise-free K_p can be expressed in terms of radar ambiguity function which is a function of the modulation function $a(t)$. K'_p is a weighted function of the volume under (or the area under a diagonal slice of, depending on the geometry case) the ambiguity function. In general, ambiguity functions which are very localized (“thumbtack-like” or concentrated near the origin $X(0, 0)$) result in the smallest K'_p values.

To illustrate the tradeoffs in selecting a transmit signal modulation scheme the ambiguity functions for three common modulation schemes are considered. These radar ambiguity functions are plotted in Fig. 6. The three modulation schemes are: 1) interrupted CW (ICW) operation where the signal is not modulated; 2) linear frequency modulation (LFM) (FM chirp) which is commonly used in radar applications including synthetic aperture radar; and 3) minimum shift keying (MSK). MSK is a form of phase modulation commonly used in communications [4]. For this application a maximal length pseudo-random data sequence is used to generate the modulation function $a(t)$. The performance is essentially independent of the particular maximal length sequence used.

The plots shown in Fig. 6 correspond to the pulse length T_p of 1.5 ms. A 66.7 kHz modulation bandwidth is used for the LFM and MSK cases. Referring to this figure, while the ambiguity functions for ICW and LFM are very broad, the MSK ambiguity function is very narrow and localized. Since K'_p is a function of the area under the ambiguity function, MSK can be expected to produce smaller net K'_p values since it has a significant value only over a very small area. To quantify this conclusion Table I summarizes the values of $Y_1(X_a)$ and $Y_2(X_a)(K'_p)$ for each modulation scheme. The values shown in Table I are normalized by $Y_1(\text{ICW})$ and correspond to

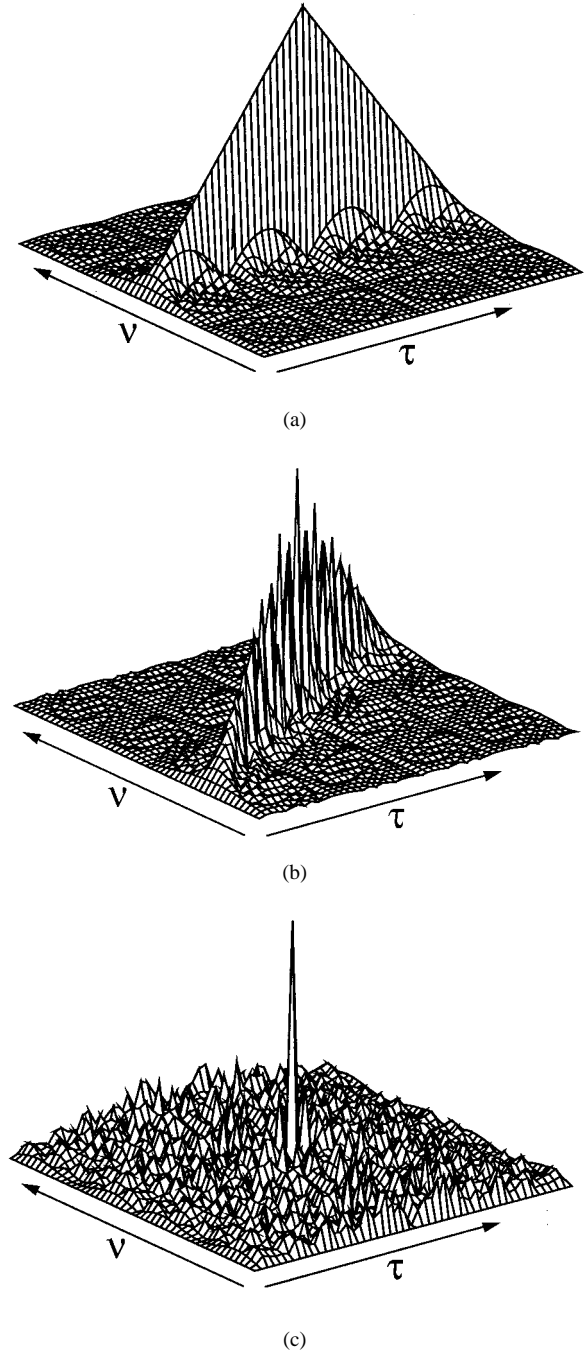


Fig. 6. The radar ambiguity function ($|X(t, \omega)|$) corresponding to (a) interrupted CW modulation, (b) LFM, and (c) MSK.

$T_c = T_p/6$ and $\omega_D = 12$ kHz. Actual K_p values for SeaWinds are given in [8].

Table I reveals that the choice of the modulation scheme affects the value of K'_p and that the resulting K'_p is dependent on the measurement geometry. ICW provides the best performance for a 0° scan angle (measurement geometry case two); however, the performance of ICW for geometry case one (90° scan angle) is not as good as LFM and MSK. Comparing the overall performance of LFM and MSK, we find that MSK provides the best performance for measurement geometry case one with only minimal degradation for case two. Since MSK

TABLE I
 K'_p FOR THE TWO SIMPLIFIED GEOMETRY CASES, $Y_1(X_a)$ AND $Y_2(X_a)$,
 NUMERICALLY COMPUTED FOR VARIOUS TRANSMIT SIGNAL MODULATION
 SCHEMES. THE VALUES SHOWN HAVE BEEN NORMALIZED BY $Y_1(ICW)$

| Modulation | $Y_1(X_a)$ | $Y_2(X_a)$ |
|------------|------------|------------|
| ICW | 1.0 | 1.0 |
| LFM | 0.9 | 1.16 |
| MSK | 0.43 | 1.05 |

can be easily generated in hardware, it was chosen for the baseline SeaWinds design [8].

K'_p for ICW is inversely proportional to the square root of the product of the pulse length and the Doppler bandwidth (the time-bandwidth product of the echo return) [see (37)]. The number of “independent looks” is thus proportional to the time-Doppler bandwidth product. Examining the radar ambiguity function (Fig. 6), we see that the ambiguity function for ICW is narrow only in the frequency dimension. In effect, only the Doppler information in the return provides “looks” when ICW is used. On the other hand, MSK is narrow in both the frequency and time dimensions, providing both range and Doppler resolution. When the Doppler and the range are coincident (geometry case two), K'_p for MSK is essentially the same as for ICW; however, when the Doppler and range are not coincident (geometry case one) K'_p for MSK is improved over ICW. In effect, MSK provides “looks” in both the Doppler and range dimensions. For geometry case one

$$K'_p(MSK) \approx \sqrt{\frac{1}{B_M T_c}} K'_p(ICW)$$

where B_M is the bandwidth of the MSK modulation. Note that to improve K'_p , $B_M > 1/T_c$. For LFM the frequency and Doppler resolution are not independent and K'_p is essentially the same as for ICW.

While increasing N_b arbitrarily will improve the noise-free K_p , K'_p , the receiver bandwidth must also be increased to accommodate the signal; however, as the receiver bandwidth is increased the noise terms in (25) become increasingly important and the total K_p increases. The total K_p will depend on the signal to noise ratio as well as the bandwidth, requiring a tradeoff between the signal modulation, the receiver bandwidth, and the total K_p . This tradeoff is considered in detail in the companion paper [8].

V. SUMMARY

Expressions for the measurement K_p for a σ^o measurement from a pencil-beam scatterometer with simple power detection have been derived. These expressions can be used for separate signal+noise and noise-only measurements as well as simultaneous measurements. The K_p expressions include transmit signal modulation and the effects of the antenna gain pattern. These K_p expressions reduce to Fisher’s analog K_p expression when the modulation is interrupted CW. Using a simplified geometry, K_p is related to the radar ambiguity function, enabling simple comparisons in K_p performance for different modulation schemes.

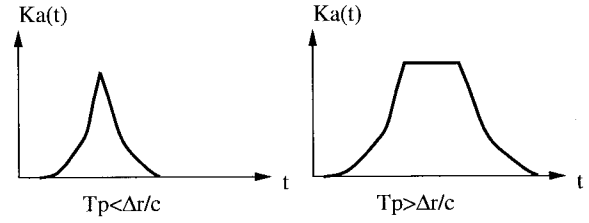


Fig. 7. The two cases for $K_a(t)$.

Based on these we conclude (1) that the radar ambiguity function approach can be useful in making first-order tradeoffs in modulation functions to minimize the noise-free K_p and (2) choosing an appropriate modulation scheme can result in improvements in K_p but (3) the amount of improvement in K_p is dependent on the measurement geometry and the scan angle.

The existence of analytic expressions for K_p permit detailed tradeoffs in the design of spaceborne scatterometer systems. Further, these expressions are needed to compute the actual measurement signal variance since the measurement K_p is required when retrieving the wind from the estimated backscatter measurements [7]. The application of these K_p equations to design tradeoffs for a spaceborne scatterometer is described in a separate paper [8].

APPENDIX A:

Interrupted CW Operation

Let us consider the single pulse K_p [(25)] for the separate measurement case when the signal is not modulated, i.e., when the transmitted signal is interrupted CW. This section demonstrates that Fisher’s K_p equation [2] is a special case of (25).

We first compute some specific results for the case of interrupted CW operation where

$$a(t) = \begin{cases} \frac{1}{\sqrt{T_p}} & 0 \leq t \leq T_p \\ 0 & \text{else.} \end{cases}$$

Depending on the length of T_p compared to the differences in time-of-flight across the footprint, $K_a(t)$ may be either triangular or trapezoidal (see Fig. 7). We will concentrate on the second case. This corresponds to $T_p \gg T_c$ where $T_c = 2\bar{r}/c$.

For this case, and using a simplified antenna gain pattern (see Section IV-A), the ramp up and ramp down times can be ignored and $K_a(t)$ can be approximated as a simple rect function of length T_p centered about the mean time-of-flight (\bar{r}/c), i.e.,

$$K_a(t) \approx \begin{cases} 1/T_p & 2\bar{r}/c \leq t \leq 2\bar{r}/c + T_p \\ 0 & \text{else.} \end{cases}$$

If the range gates are set so that the integration in (16) exactly covers the “flat top” of $K_a(t)$ then $a_1 \approx T_p/T_r$ where $T_r = T_2 - T_1$ is the range gate length.

Computing V is somewhat more difficult. For the interrupted CW case with the simplified antenna gain $J_a(t, \tau)$ can

be written as

$$J_a(t, \tau) = \frac{1}{A_c^2 T_p^2} \int \cdots \int p(t - 2r/c) p(\tau - 2r/c) \\ \cdot p(t - 2r'/c) p(\tau - 2r'/c) \\ \cdot A_r(r, \omega_d) A_r(r', \omega'_d) \\ \cdot e^{-j(\omega_d - \omega'_d)(t - \tau)} dr d\omega_d dr' d\omega'_d$$

where $p(t) = \sqrt{T_p} a(t)$. For $T_p \gg T_c$, if we consider only values of t and τ within the ‘‘flat top’’ period of the return $J_a(t, \tau)$ can be approximated as

$$J_a(t, \tau) \approx \frac{1}{A_c^2 T_p^2} \int \cdots \int A_r(r, \omega_d) A_r(r', \omega'_d) \\ \cdot e^{-j(\omega_d - \omega'_d)(t - \tau)} dr d\omega_d dr' d\omega'_d.$$

Note that $J_a(t, \tau)$ is only a function of the time difference between t and τ , i.e., $J(t - \tau) = J_a(t, \tau)$.

In principle we have to evaluate $J(t)$ separately for each illumination geometry. Because the exact expressions are very complicated, let us again assume a simplified geometry (Fig. 5). Then, $J(t)$ can be written as

$$J(t) = \frac{1}{T_p^2 \omega_D^2} \int_{\omega_n}^{\omega_x} \int_{\omega_n}^{\omega_x} e^{-j(\omega_d - \omega'_d)t} d\omega_d d\omega'_d \\ = \frac{1}{T_p^2 \omega_D^2} \frac{2}{t^2} [1 - \cos(\omega_D t)]$$

which produces

$$V = \int_{-T_r}^{T_r} (T_r - |\alpha|) \frac{1}{T_p^2 \omega_D^2} \frac{2}{\alpha^2} [1 - \cos(\omega_D \alpha)] d\alpha.$$

Performing this integration and assuming a large time-bandwidth product $T_r \omega_D$ it can be shown that

$$V \approx 2\pi T_r \omega_D \frac{1}{T_p^2 \omega_D^2}.$$

For our simplified antenna pattern and geometry and integrating over the flat top portion of the return with the ramp up and down times ignored, $L_a(t, \tau)$ reduces to

$$L_a(t, \tau) = L(t - \tau) = \frac{1}{T_p \omega_D} \int_{\omega_n}^{\omega_x} e^{-j\omega_d(t - \tau)} d\omega_d.$$

Performing the integration,

$$L(x) = 2 \frac{1}{T_p \omega_D} e^{-j\omega_c x} \frac{1}{x} \sin(\omega_D x / 2).$$

Then

$$U = \frac{2}{T_r} L_c(T_r)$$

where

$$L_c(x) = \int_{-x}^x (x - |\alpha|) \operatorname{Re}[L(\alpha)] \operatorname{sinc}(2B_r \alpha) d\alpha.$$

Simplifying, and using the substitution $y = \alpha/x$,

$$L_c(x) = \frac{4}{T_p \omega_d} x^2 \int_0^1 (1 - y) \cos(\omega_c x y) \\ \cdot \frac{\sin(\omega_D x y / 2)}{x y} \frac{\sin 2\pi B_r x y}{2\pi B_r x y} dy$$

which can be expressed as [2]

$$L_c(x) = \frac{1}{4\pi B_r} \left[- \left(\frac{\omega_D / 2 + \omega_c - 2\pi B_r}{2} x \right)^2 \right. \\ \cdot I \left(\frac{\omega_D / 2 + \omega_c - 2\pi B_r}{2\pi} x \right) \\ + \left(\frac{\omega_D / 2 + \omega_c + 2\pi B_r}{2} x \right)^2 \\ \cdot I \left(\frac{\omega_D / 2 + \omega_c + 2\pi B_r}{2\pi} x \right) \\ - \left(\frac{\omega_D / 2 - \omega_c - 2\pi B_r}{2} x \right)^2 \\ \cdot I \left(\frac{\omega_D / 2 - \omega_c - 2\pi B_r}{2\pi} x \right) \\ + \left(\frac{\omega_D / 2 - \omega_c + 2\pi B_r}{2} x \right)^2 \\ \left. \cdot I \left(\frac{\omega_D / 2 - \omega_c + 2\pi B_r}{2\pi} x \right) \right].$$

For large time-bandwidth products $x\omega_D \gg 1$ this becomes

$$L_c(x) \approx \frac{2}{T_p \omega_d} \pi x.$$

It follows that,

$$U = \frac{2}{T_p B_D}$$

where $B_D = \omega_D / 2\pi$ is the Doppler bandwidth in Hz.

Let us now define the signal-to-noise ratio (SNR) as the ratio of the return echo energy ($E_s = a_1 \mathcal{E}[C_s]$) to the noise power over the signal measurement bandwidth and range gate length, i.e.,

$$\text{SNR} = \frac{E_s}{E_n} = \frac{a_1 \mathcal{E}[C_s]}{E_n} = \frac{1}{S}.$$

Assuming a large time-bandwidth product, $I(x) \approx 1/x$ and the measurement variance, (23), for the interrupted CW case becomes

$$\operatorname{var}[\widehat{E}_s] = a_1^2 E_s^2 \left\{ T_r B_D \left(\frac{1}{T_p B_D} \right)^2 + \frac{1}{T_p B_D} \frac{2}{\text{SNR}} \right. \\ \left. + \frac{1}{\text{SNR}^2} \frac{1}{T_r B_r} \left(1 + \frac{T_r B_r}{T_n B_n} \right) \right\}.$$

For an optimally chosen range gate and ignoring the rise and fall time of the pulse $T_p \approx T_r$. It follows that $a_1 \approx 1$. We will set $B_r = B_D$. It follows that K_p for the simplified interrupted CW case is

$$K_p[E_s] = \frac{1}{\sqrt{T_r B_r}} \left\{ 1 + \frac{2}{\text{SNR}} \right. \\ \left. + \frac{1}{\text{SNR}^2} \left[1 + \frac{B_r T_r}{T_n B_n} \right] \right\}^{1/2}. \quad (36)$$

which is equivalent to the analog K_p expression of Fisher (see (48) in [2]). Thus, (25) reduces to the Fisher's K_p when

the modulation is interrupted CW. The noise-free K_p, K'_p , for this case is

$$K'_p = \frac{1}{\sqrt{T_r B_r}} \quad (37)$$

APPENDIX B:

K_p for Simultaneous Measurements with Overlapping Bandwidths

In deriving (25), it was assumed that independent measurements of the signal+noise, C_{sn} , and of the noise-only, C_{no} , were made. Let us now consider the case when the signal+noise and noise-only measurements are made simultaneously and the noise-only measurement bandwidth includes the signal+noise measurement bandwidth (the SMBW case) (see Fig. 2). The “noise-only” measurement now includes a signal component and is, in reality, a signal+noise measurement. However, the noise-only measurement bandwidth is much larger than the signal+noise measurement bandwidth, i.e., $B_n \gg B_r$. We will denote the “noise-only” measurement C_{no} for this case by C'_{no} . For simplicity we will set $T_3 = T_1$ and $T_4 = T_2$ (thus, $T_n = T_r$) though this is not a requirement.

To simplify notation the noise in the signal+noise measurement is denoted as $\nu_s(t) = \nu(t) * h(t)$ and the noise in the noise-only measurements as $\nu_n(t) = \nu(t) * h_n(t)$. Using this notation, the received signal+noise $\xi_{sn}(t)$ and “noise-only” $\xi_{no}(t)$ signals are

$$\begin{aligned} \xi_{sn}(t) &= \xi_s(t) + \nu_s(t) \\ \xi_{no}(t) &= \xi_s(t) + \nu_n(t). \end{aligned}$$

Assuming that $h_n(t)$ is wide enough to not affect the signal, the noise-only measurement is

$$C'_{no} = \int_{T_3}^{T_4} |\xi_s(t) + \nu_n(t)|^2 dt.$$

For this case the signal energy is estimated by [compare (8)]

$$\widehat{E}_s = a'_1 C_{sn} - b'_1 C'_{no} \quad (38)$$

where the coefficient a'_1 and b'_1 are given by

$$\begin{aligned} a'_1 &= a_1 \frac{B_n}{B_n - B_r} \\ b'_1 &= a_1 \frac{B_r}{B_n - B_r}. \end{aligned}$$

It is easily shown that $\mathcal{E}[\widehat{E}_s] = E_s$.

Following the approach given in the main text [see (11)], C'_{no} may be expressed in terms of the signal-only energy C_s [defined in (12)], a noise-component C'_n , and a cross-product, C'_c

$$C'_{no} = C_s + C'_c + C'_n$$

where

$$\begin{aligned} C'_c &= \int_{T_1}^{T_2} [\xi_s(t)\nu_n^*(t) + \xi_s^*(t)\nu_n(t)] dt \\ C'_n &= \int_{T_1}^{T_2} |\nu_n(t)|^2 dt. \end{aligned}$$

It can be easily shown that

$$\begin{aligned} \mathcal{E}[C'_c] &= 0 \\ \mathcal{E}[C'_n] &= 2B_n T_n \frac{n_0}{2} = 2B_n T_r \frac{n_0}{2} \\ \text{var}[C'_{no}] &= \text{Var}[C_s] + \text{Var}[C'_c] + \text{Var}[C'_n] \end{aligned}$$

where $\text{var}[C_s]$ is given in (17) and

$$\text{var}[C'_c] = E_s^2 S U' \quad (39)$$

$$\text{var}[C'_n] = 2E_s^2 S^2 \frac{B_n^2}{B_r^2} I(2B_n T_r) \quad (40)$$

where U' is defined in the same way as U in (15) but with B_r replaced with B_n .

For later use we compute several expected values. Noting the independence of the signal and noise

$$\mathcal{E}[C_s C_n] = 2B_r T_r \frac{n_0}{2} \frac{E_s}{a_1} = E_s^2 \frac{S}{a_1} \quad (41)$$

$$\mathcal{E}[C_s C'_n] = 2B_n T_r \frac{n_0}{2} \frac{E_s}{a_1} = E_s^2 \frac{S}{a_1} \frac{B_n}{B_r} \quad (42)$$

The noise-component of the noise-only signal $\nu_n(t)$ can be expressed as the sum of the noise-only portion of the signal+noise $\nu_s(t) = \nu(t) * h(t)$ and an independent noise component $\nu_0(t)$ ($\nu_0(t) = \nu_n(t) - \nu_s(t)$). Noting the independence of $\nu_s(t)$ and $\nu_0(t)$ it follows that

$$\mathcal{E}[\nu_s(t)\nu_n^*(\tau)] = \mathcal{E}[\nu_s(t)\nu_s^*(\tau)] \quad (43)$$

$$= R_{\nu_s}(t - \tau) = 2B_r \frac{n_0}{2} \text{sinc}(2B_r[t - \tau]). \quad (44)$$

Then, since $\nu_s(t), \nu_n(t)$, and $\nu_0(t)$ are zero mean,

$$\begin{aligned} \mathcal{E}[|\nu_s(t)|^2 |\nu_n(\tau)|^2] &= \mathcal{E}[|\nu_s(t)|^2 |\nu_s(\tau)|^2] \\ &\quad + \mathcal{E}[|\nu_s(t)|^2] \mathcal{E}[|\nu_0(\tau)|^2] \end{aligned}$$

from which it follows that

$$\mathcal{E}[C_n C'_n] = E_s^2 S^2 [2I(2B_r T_r) + B_n/B_r]. \quad (45)$$

Noting that the expected value of a third-order product of zero mean Gaussian random processes is zero it follows that

$$\begin{aligned} \mathcal{E}[C_c C'_n] &= \int_{T_1}^{T_2} \int_{T_1}^{T_2} \mathcal{E}[\{\xi_s(t)\nu_s^*(t) \\ &\quad + \xi_s^*(t)\nu_s(t)\} |\nu_n(\tau)|^2] dt d\tau = 0. \end{aligned} \quad (46)$$

Similarly,

$$\mathcal{E}[C'_c C_n] = 0 \quad (47)$$

$$\mathcal{E}[C_s C'_c] = 0 \quad (48)$$

$$\mathcal{E}[C_s C_c] = 0. \quad (49)$$

Using (43), the fact that the noise is real, and noting that $\mathcal{E}[\xi_s(t)\xi_n(\tau)] = 0$,

$$\begin{aligned} \mathcal{E}[\{\xi_s(t)\nu_n^*(t) + \xi_s^*(t)\nu_n(t)\} \cdot \{\xi_s(\tau)\nu_n^*(\tau) + \xi_s^*(\tau)\nu_n(\tau)\}] \\ = 2E_s \text{Re}[L_a(t, \tau)] R_{\nu_s}(t - \tau) \end{aligned}$$

and

$$\mathcal{E}[C_c C'_c] = E_s^2 S U. \quad (50)$$

Defining $V' = a_1^{-2}$ we can express $\mathcal{E}[C_s^2]$ as

$$\mathcal{E}[C_s^2] = X^2 \sigma^{o2} (V' + V) = E_s^2 (V' + V). \quad (51)$$

Combining (41), (50), (42), (49), (48), (51), (42), and (45), we obtain

$$\begin{aligned} \mathcal{E}[C_{sn} C'_{no}] &= E_s^2 \left[V' + V + SU + S \left(1 + \frac{B_n}{B_r} \right) \right. \\ &\quad \left. + 2S^2 (I(2B_r T_r) + B_n/B_r) \right]. \end{aligned} \quad (52)$$

It is easily shown that

$$\begin{aligned} \mathcal{E}[C_{sn}] &= E_s/a_1 + 2T_r B_r \frac{n_0}{2} \\ \mathcal{E}[C'_{no}] &= E_s/a_1 + 2T_r B_n \frac{n_0}{2} \end{aligned}$$

from which it follows that

$$\mathcal{E}[C_{sn}] \mathcal{E}[C'_{no}] = E_s^2 \left[V' + S \left(1 + \frac{B_n}{B_r} \right) + S^2 \frac{B_n}{B_r} \right].$$

Combining this result with (52) we obtain

$$\begin{aligned} \mathcal{E}[C_{sn} C'_{no}] - \mathcal{E}[C_{sn}] \mathcal{E}[C'_{no}] \\ = E_s^2 \{ V + SU + S^2 2I(2B_r T_r) \}. \end{aligned} \quad (53)$$

Finally, combining (14), (17), (20), (38)–(40), and (53) and performing some tedious algebra it can be shown that

$$\begin{aligned} \text{var}[\widehat{E}_s^2] &= a_1^2 E_s^2 \left\{ V + S \left[U + (U' - U) \frac{B_r^2}{(B_n - B_r)^2} \right] \right. \\ &\quad \left. + 2S^2 \left[I(2B_r T_r) \left(1 - \frac{B_r^2}{(B_n - B_r)^2} \right) \right. \right. \\ &\quad \left. \left. + \frac{B_n^2}{(B_n - B_r)^2} I(2B_n T_r) \right] \right\}. \end{aligned}$$

Since $\mathcal{E}[\widehat{E}_s] = E_s$ it follows that for independent pulses K_p for the SMBW case is

$$\begin{aligned} K_p[\widehat{E}_s \text{ SMBW}] &= \frac{a_1}{\sqrt{N_p}} \left\{ V + S \left[U + (U' - U) \frac{B_r^2}{(B_n - B_r)^2} \right] \right. \\ &\quad \left. + 2S^2 \left[I(2B_r T_r) \left(1 - \frac{B_r^2}{(B_n - B_r)^2} \right) \right. \right. \\ &\quad \left. \left. + \frac{B_n^2}{(B_n - B_r)^2} I(2B_n T_r) \right] \right\}^{1/2} \end{aligned} \quad (54)$$

which can be expressed in the form of (26).

Comparing the K_p for the simultaneous, overlapping bandwidth measurement case [(26)] with the K_p for the separate case [(25)] we note the presence of an additional term (W) due to the presence of the signal in the noise-only measurement bandwidth. (Note that W depends on the SNR via U and U' .) W arises due to cross-products of the signal and noise from the signal+noise and noise-only measurements. W is positive and tends to increase K_p . However, this increase can be minimized by choosing $B_n \gg B_r$. Q_1 and Q_2 arise due to the different scaling factors (a_1' and b_1') used for the simultaneous measurements and the correlation of the noise in the signal bandwidth.

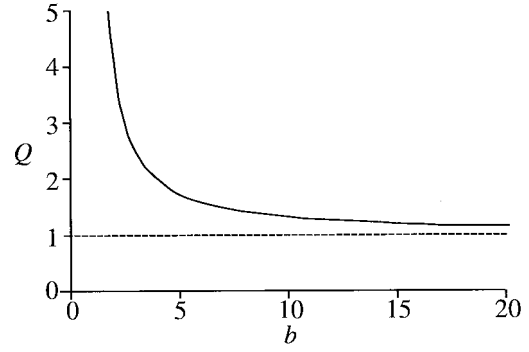


Fig. 8. Plot of Q versus $b = B_n/B_r$. Note that as b increases, $Q \rightarrow 1$.

Note that for large time bandwidth products ($B_r T_r \gg 1$ and $B_n T_r \gg 1$), $I(p) \rightarrow 1/p$. Then,

$$Q_1 I(2B_r T_r) + Q_2 I(2B_n T_r) \approx \frac{1}{2B_r T_r} Q$$

where (remembering that $B_n > B_r$)

$$Q = \frac{B_n^2 + B_n B_r - 2B_r^2}{(B_n - B_r)^2} = \frac{b^2 - b - 2}{(b - 1)^2}$$

where $b = B_n/B_r$ is the noise-only to signal+noise bandwidth ratio. Note that as b is increased, $Q \rightarrow 1$ (See Fig. 8). Thus, the noise term is larger for the overlapping case but the difference between the cases is reduced as b is increased.

From these results we conclude that while the K_p is larger for the SMBW case, maximizing $B_n \gg B_r$ minimizes K_p and, for very large $B_n \gg B_r$, the K_p for the two cases converge. For large time bandwidth products, (54) can be approximated by

$$\begin{aligned} K_p[\text{SMBW}] &\approx \frac{a_1}{\sqrt{N_p}} \left\{ V + S \left[U + (U' - U) \frac{B_r^2}{(B_n - B_r)^2} \right] \right. \\ &\quad \left. + S^2 \frac{B_n^2 + B_n B_r - 2B_r^2}{(B_n - B_r)^2} \right\}^{1/2}. \end{aligned} \quad (55)$$

When the modulation is interrupted CW, (55) can be approximated by Fisher's K_p . Following the procedure outlined in Appendix A it can be shown that

$$U' = \frac{2}{T_r B_D} \frac{B_D}{B_n}.$$

Substituting this and the expressions for V, U , and a_1 derived in Appendix A into (54) we obtain

$$\begin{aligned} K_p[\text{ICW, SMBW}] &= \frac{1}{\sqrt{T_r B_D N_p}} \left\{ 1 + \frac{2}{\text{SNR}} \left[1 - \frac{B_D^2}{B_n(B_n - B_D)} \right] \right. \\ &\quad \left. + \frac{1}{\text{SNR}^2} \frac{B_n^2 + B_n B_r - 2B_r^2}{(B_n - B_r)^2} \right\}^{1/2}. \end{aligned} \quad (56)$$

This result may be compared with Fisher's K_p , which applies only to interrupted CW modulation with true independent

signal+noise and noise-only measurements, given in (36). (Remembering that $T_r = T_n$.) Note the additional term in the $2/\text{SNR}$ product term and the changes to the $1/\text{SNR}^2$ term. These arise due to the fact that the noise in the signal+noise measurement bandwidth is not independent of the noise in the noise-only measurement, resulting in a somewhat higher K_p .

REFERENCES

- [1] C-Y. Chi, D. G. Long, F. K. Li, "Radar backscatter measurement accuracies using digital doppler processors in spaceborne scatterometers," *IEEE Trans. Geosci. Remote Sensing*, vol. GE-24, May 1986.
- [2] R. Fisher, "Standard deviation of scatterometer measurements from space," *IEEE Trans. Geosci. Electron.*, vol. GE-10, Apr. 1972.
- [3] M. H. Freilich, D. G. Long, and M. W. Spencer, "SeaWinds: A scanning scatterometer for ADEOS II—Science overview," in *Proc. Int. Geosci. Remote Sensing Symposium*, Pasadena, CA, Aug. 8–12, 1994, pp. 960–963.
- [4] S. Haykin, *Communication Systems*. New York: Wiley, 2nd ed., 1983.
- [5] D. G. Long, C-Y Chi, and F. K. Li, "The design of an onboard digital doppler processor for a spaceborne scatterometer," *IEEE Trans. Geosci. Remote Sensing*, vol. 26, pp. 869–878, Nov. 1988.
- [6] D. G. Long, M. H. Freilich, D. F. Leotta, D. E. Noon, "A scanning scatterometer for the Eos polar platform," in *Proc. Int. Geosci. Remote Sensing Symp.*, Washington, D.C., May 20–24, 1990, pp. 2447–2450.
- [7] F. Naderi, M. H. Freilich, and D. G. Long, "Spaceborne radar measurement of wind velocity over the ocean—An overview of the NSCAT scatterometer system," *Proc. IEEE*, pp. 850–866, vol. 79, June 1991.
- [8] M. W. Spencer and D. G. Long, "Tradeoffs in the design of a spaceborne scanning pencil-beam scatterometer: Application to SeaWinds," this issue, pp. 115–127.
- [9] F. T. Ulaby, R. K. Moore, and A. K. Fung, *Microwave Remote Sensing—Active and Passive*. Reading, MA: Addison-Wesley, 1981.



David Long (S'80–M'89) received the Ph.D. degree in electrical engineering from the University of Southern California, Los Angeles, in 1989.

From 1983 to 1990, he worked for NASA's Jet Propulsion Laboratory where he developed advanced radar remote sensing systems. While at JPL he was the Senior Project Engineer on the NASA Scatterometer (NSCAT) project. He is currently an Associate Professor in the Electrical and Computer Engineering Department, Brigham Young University, Provo, UT, where he teaches upper division and graduate courses in communications, microwave remote sensing, radar, and signal processing. He is the principle investigator on several NASA-sponsored interdisciplinary research projects in remote sensing including innovative radar systems, spaceborne scatterometry of the ocean and land, and modeling of atmospheric dynamics. His research interests include microwave remote sensing, radar theory, space-based sensing, estimation theory, computer graphics, signal processing, and mesoscale atmospheric dynamics. He is a member of the NSCAT Science Working Team. He has numerous publications in signal processing and radar scatterometry.



Michael W. Spencer received the B.S. degree in physics from the College of William and Mary, Williamsburgh, VA, in 1985, the M.S. in planetary science from the California Institute of Technology in 1987, and the M.S. in electrical engineering from the University of Southern California in 1995.

From 1987 to 1990 he was employed at the Aerospace Corporation where he was involved in the modeling and analysis of advanced meteorological and surveillance satellite systems. Since 1990, he has been employed at the Jet Propulsion Laboratory where he has worked on the conceptualization, system design, performance simulation, and validation of radar remote sensing instruments. Mr. Spencer is a member of Phi Beta Kappa.